Open access • Journal Article • DOI:10.1029/2008JD011532

Ice nuclei emissions from biomass burning — Source link

Markus D. Petters, Matthew T. Parsons, Matthew T. Parsons, Anthony J. Prenni ...+10 more authors

Institutions: Colorado State University, University of Alberta, University of Manchester, United States Department of Agriculture ...+1 more institutions

Published on: 16 Apr 2009 - Journal of Geophysical Research (John Wiley & Sons, Ltd)

Topics: Ice nucleus and Cloud condensation nuclei

JOURNAL OF GEOPHYSICAL RESEARCH, VOL. 114, D07209, doi:10.1029/2008JD011532, 2009

Ice nuclei emissions from biomass burning

Markus D. Petters,[1] Matthew T. Parsons,[1,2] Anthony J. Prenni,[1] Paul J. DeMott,[1] Sonia M. Kreidenweis,[1] Christian M. Carrico,[1] Amy P. Sullivan,[1] Gavin R. McMeeking,[1,3] Ezra Levin,[1] Cyle E. Wold,[4] Jeffrey L. Collett Jr.,[1] and Hans Moosmüller[5]

Received 25 November 2008; revised 3 February 2009; accepted 11 February 2009; published 15 April 2009.

[1] Biomass burning is a significant source of carbonaceous aerosol in many regions of the world. When present, biomass burning particles may affect the microphysical properties of clouds through their ability to function as cloud condensation nuclei or ice nuclei. We report on measurements of the ice nucleation ability of biomass burning particles performed on laboratory-generated aerosols at the second Fire Lab at Missoula Experiment. During the experiment we generated smoke through controlled burns of 21 biomass fuels from the United States and Asia. Using a Colorado State University continuous flow diffusion chamber, we measured the condensation/immersion freezing potential at temperatures relevant to cold cumulus clouds (−30°C). Smokes from 9 of the 21 fuels acted as ice nuclei at fractions of 1:10,000 to 1:100 particles in at least one burn of each fuel; emissions from the remaining fuels were below the ice nuclei detection limit for all burns of each fuel. Using a bottom-up emission model, we estimate that smokes that emit ice nuclei fractions exceeding 1:10,000 particles can perturb ice nuclei concentrations on a regional scale.

Citation: Petters, M. D., et al. (2009), Ice nuclei emissions from biomass burning, *J. Geophys. Res.*, *114*, D07209, doi:10.1029/2008JD011532.

1. Introduction

[2] Combustion processes produce large quantities of aerosol particles globally and represent major contributions to global aerosol optical depth [*Robertson et al.*, 2001]. Biomass burning emissions make up a significant fraction of these particles, representing 7% of total particulate matter emissions by weight on a global annual basis [*Andreae*, 1991] and 78% of the total carbonaceous aerosol burden [*Reddy and Boucher*, 2004]. In the United States, biomass burning (summer wildfires, other fires, residential biofuel, and industrial biofuel) contributes approximately 50% of the annual mean total carbonaceous aerosol mass concentration and accounts for 20–30% of total observed fine aerosol concentrations [*Park et al.*, 2007]. Biomass burning particles impact climate directly through the extinction properties of the particles themselves [*Yu et al.*, 2006] and indirectly by impacting cloud cover [*Koren et al.*, 2004; *Lin et al.*, 2006] and precipitation [*Lin et al.*, 2006], although the magnitude and direction of these effects appear to depend on cloud type. The presence of elevated aerosol concentrations due to smoke also can delay the onset of warm cloud precipitation and invigorate convection, transporting water to supercooled temperatures [*Andreae et al.*, 2004] where ice nucleation can occur. The presence of ice in clouds can initiate precipitation [*Intergovernmental Panel on Climate Change*, 2007], influence cloud lifetime and areal coverage, impact cloud optical depth and radiative forcing [*McFarquhar and Cober*, 2004; *McFarquhar et al.*, 2007; *Zuidema et al.*, 2005], and influence atmospheric chemical reactions [see, e.g., *Abbatt*, 2003, and references therein].

[3] Ice nucleation can produce either mixed-phase clouds (containing both ice and liquid) or completely glaciated clouds. For temperatures from 0 to −36°C, primary ice formation is the result of heterogeneous ice nucleation. Heterogeneous ice nucleation can occur via multiple freezing mechanisms: deposition, condensation, immersion, or contact [*Vali*, 1985]. Nucleation usually occurs at active sites that reside on water-insoluble surfaces that are exposed to liquid water (immersion, condensation, and contact) or to air that is supersaturated with respect to ice (deposition). These active sites are hypothesized to be related to surface defects in the crystalline structure of the ice-nucleating agent [*Vonnegut*, 1947]. Long-chain alcohols [*Gavish et al.*, 1990] also can initiate ice formation by forming self-assembled monolayers on the surface of supercooled droplets. Cyclic hydrocarbons such as 1,5-dihydroxynaphthalene

[1]Department of Atmospheric Science, Colorado State University, Fort Collins, Colorado, USA.
[2]Now at Departments of Chemistry and Electrical Engineering, University of Alberta, Edmonton, Alberta, Canada.
[3]Now at Center for Atmospheric Science, University of Manchester, Manchester, UK.
[4]Fire Sciences Laboratory, U.S. Department of Agriculture Forest Service, Missoula, Montana, USA.
[5]Desert Research Institute, Nevada System of Higher Education, Reno, Nevada, USA.

0148-0227/09/2008JD011532$09.00

Table 1. Fuels Used in This Study[a]

Southeastern U.S. Fuels		Western U.S. Fuels		Miscellaneous Fuels	
Fuel Name	State	Fuel Name	State	Fuel Name	Region/Country
Common reed (plant) *Phragmites australis*	CA	ceanothus (plant) *Ceanothus crassifolius*	CA	charcoal (bricks)	Asia
Gallberry (plant) *Ilex glabra*	MS	chamise (plant) *Adenostoma fasciculatum*	CA	rice straw (plant) *Oryza*	Taiwan
Hickory (leaves) *Carya*	NC	Douglas fir (branches/needles) *Pseudotsuga menziesii*	MT		
Longleaf pine (needles) *Pinus palustris*	MS	duff (uppermost layer of soil with live and dead feather moss, *Pleurozium schreberi*)	AK		
Needlegrass rush (plant) *Juncus roemerianu*	FLNC	manzanita (plant) *Arctostaphylos glandulosa*	CA		
Oak (leaves) *Quercus laevis*	NC	ponderosa pine (needles) *Pinus ponderosa*	MT		
Palmetto (leaves) *Serenoa repens*	FLMS	sagebrush (plant) *Artemisia tridentate*	MTUT		
Swamp saw grass (plant) *Cladium mariscus jamaicense*	MSNC	black spruce (plant) *Picea A. Dietr.*	AK		
Titi (plant) *Cyrilla racemiflora*	FL				
Wax myrtle (plant) *Myrica cerifera*	MS				
Wire grass (plant) *Aristida beyrichiana*	MS				

[a]Fuel names are given as common name, part of fuel burned (in parentheses), and scientific name (in italics). The term "plant" denotes that a part of the plant, representative of its aboveground biomass, was burned.

and phloroglucinol [*Langer et al.*, 1978] have been shown to nucleate ice. A particle that causes a droplet to freeze is typically referred to as a heterogeneous ice nucleus (IN).

[4] Biomass burning plumes are capable of reaching high altitudes and thus experience low temperatures [*Andreae et al.*, 2004]. These particles may contain sites active in ice nucleation because of the large fraction of insoluble components in these aerosol particles [*Diehl et al.*, 2006, 2007], but this conjecture has not been verified to date. Remote sensing data from the Amazon Basin [*Lin et al.*, 2006] and boreal forests in Alaska [*Sassen and Khvorostyanov*, 2008] provide inferential evidence for smoke particles affecting ice processes in clouds. Ambient measurements of Arctic aerosol processed in an ice nuclei instrument [*Prenni et al.*, 2009] also suggest an influence of biomass burning smoke on IN concentrations. Of particular interest is the role of biomass burning soot [*Karcher et al.*, 2007]. Laboratory studies have considered ice nucleation on several types of soot particles [*DeMott*, 1990; *Diehl and Mitra*, 1998; *Dymarska et al.*, 2006; *Gorbunov et al.*, 2001] and found that combustion soot is unlikely to undergo deposition ice nucleation but suggested a potential for combustion soot particles to undergo immersion or condensation freezing. Furthermore, black carbon is sometimes enhanced in the ice crystals when compared to interstitial and cloud droplet residuals in mixed-phase clouds, and this observation has led to speculation that black carbon particles may preferentially serve as ice nuclei [*Cozic et al.*, 2008]. To date, no laboratory data on ice nuclei emissions from biomass burning are available.

[5] Here we report on the role of biomass burning particles as IN through a series of controlled burns at the U.S. Department of Agriculture Forest Service Fire Sciences Laboratory, as part of the second Fire Lab at Missoula Experiment (FLAME II). Twenty-one fuels were selected for this study, representative of those burned in wild and prescribed fires throughout the western and southeastern United States, as well as rice straw and charcoal commonly associated with agricultural and domestic burning, respectively. The fuels used in this study are listed in Table 1 along with the state, region, or country where each fuel was collected. Where applicable, both common and scientific names are given. We tested the ability of smoke particles from each burn to nucleate ice as condensation/immersion freezing nuclei at -30°C. These measurements were carried out using one version of the Colorado State University continuous flow diffusion chamber (CFDC). Using a series of ancillary measurements that characterize the fuels, combustion conditions, gas and particulate emissions, aerosol chemical composition, and aerosol hygroscopicity, we explore statistical links between IN emissions and these properties.

2. Experimental Procedure

[6] The FLAME II study was carried out in May and June 2007 at the U.S. Department of Agriculture Forest Service Fire Sciences Lab in Missoula, Montana. An overview of this study with details of the combustion facility, fuels used, combustion, sampling, and analytical procedures has been given by *McMeeking* [2008]. Biomass fuels were burned in a combustion chamber that features a volume of approximately 3400 m^3 and an exhaust stack that can be used to vent the chamber (Figure 1). A platform surrounding the exhaust stack 16 m above ground provides access to multiple sampling ports into the exhaust stack. Prior to the burns, 30–500 g of fuel were placed on a ceramic tile lined with resistive heating wire sheathed in a Thermeez 395 woven ceramic sleeving that was soaked in 15 g of ethanol. The ceramic tile was placed on a Mettler PM34 microbalance and then a voltage was applied to the heating wire, igniting the ethanol fumes and resulting in a uniform ignition of the fuel bed. The combustion emissions were pulled into the exhaust stack directly above the fuel bed. A 1.25 inch inner diameter stainless steel tube was inserted into the center of the exhaust stack at a height of approximately 16 m above the fuel bed. This stainless steel sampling tube, approximately 20 m in length, was connected to a 200 L volume stainless steel sampling drum. A high-volume air pump (300 L min^{-1}) pulled combustion emissions from the exhaust stack into the sampling drum to store the aerosol for a subsequent sampling period lasting 20–30 min. The sampling period was synchronized with those used for the determination of the emission parameters listed in Table 2, except for the filter measurements, which were integrated over the entire burn. After collecting com-

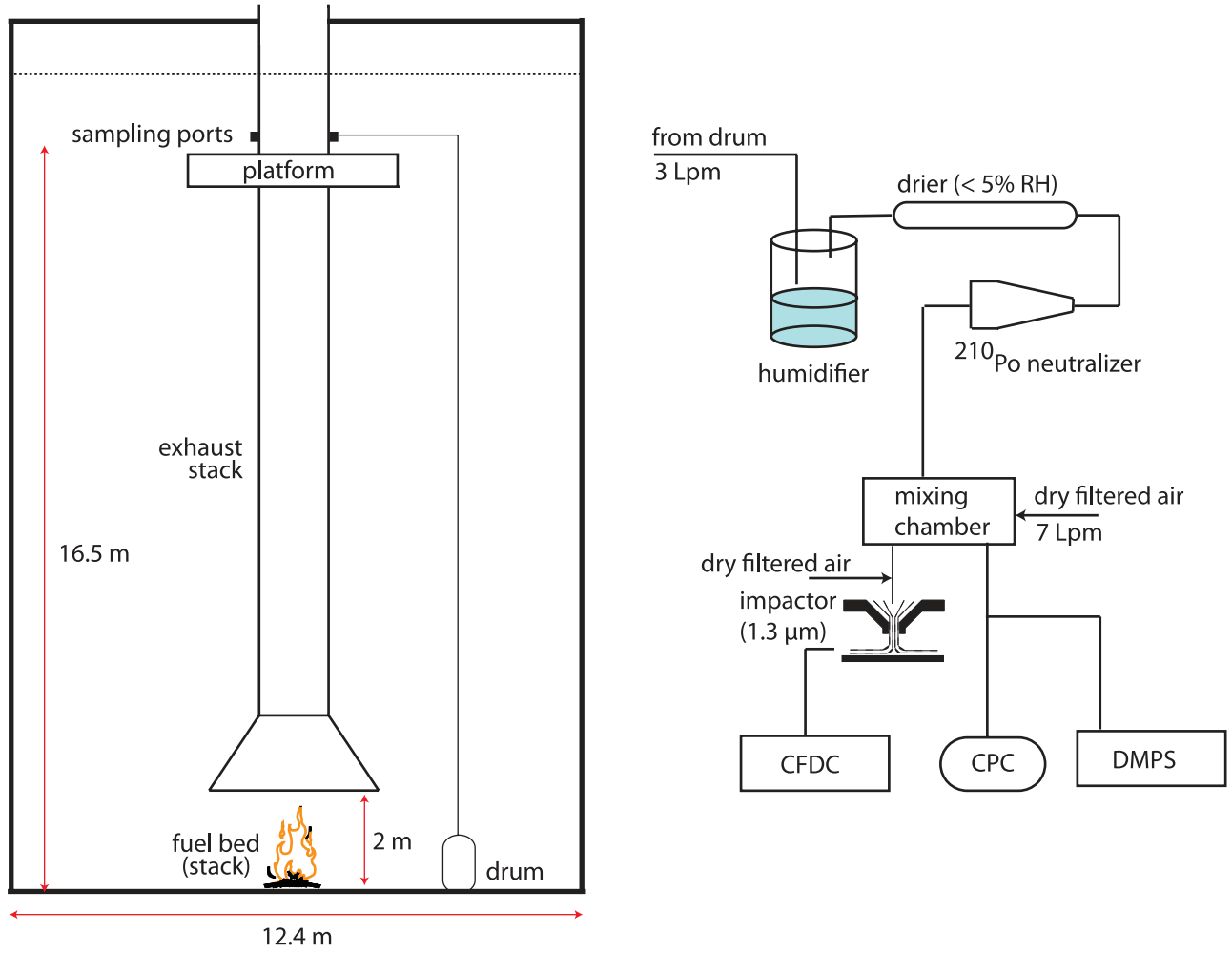

Figure 1. Schematic of the experimental setup. (left) Schematic of the Missoula Fire Sciences Laboratory. (right) Aerosol sampling strategy. Lpm, liters per minute.

bustion emissions, the inlet to the drum was sealed, and the outlet was connected to a preconditioning system that drew a 3 L min^{-1} sample from the drum. During measurements, the drum was open to the room through a high-efficiency particulate air (HEPA) filter to prevent depressurization of the drum. Particle concentrations in the drum typically exceeded 500,000 cm^{-3}, measured using an ultrafine condensation particle counter (TSI counter 3776). At those concentrations, particles rapidly coagulated and were lost to the walls, leading to a decrease in number concentration over the 20–30 min sampling period.

[7] The soot fraction of fresh combustion particles consists of fractal-like chain aggregates with a three-dimensional mass fractal dimension of ~1.75, and their aerodynamic size can vary significantly from their geometric size [*Chakrabarty et al.*, 2006]. Transmission electron microscopy tests W. P. Arnott, personal communication, 2007) showed that the hygroscopic combustion particles collapsed to reproducible sizes after wetting and subsequently drying the particles. To improve the consistency of the particle size measurements, the sample flow was humidified to >95% relative humidity (RH) and then dried to RH < 5% (Figure 1). The wetting-drying cycle, however, possibly destroyed available sites for deposition ice nucleation, and therefore, we do not report ice nucleation data below water saturation. The conditioned polydisperse size distribution was diluted with dry, filtered air in an 11 L volume stainless mixing chamber, and the sample flow was split to a differential mobility particle sizer (DMPS) to measure the size distribution (DMPS consisting of a TSI 3080 differential mobility analyzer (DMA) and 3010 condensation particle counter (CPC)), to a condensation particle counter to obtain total particle concentrations (TSI, model 3010, detects particles with $D > 15$ nm), and to a CFDC to measure IN concentrations. Figure 2 shows an example number size distribution measured by the DMPS. This instrument measured the size distribution over the range $30 < D < 300$ nm. Number mode diameters during the study ranged from 80 to 200 nm. Ambient data show correlations between ice nuclei and aerosol number exceeding a threshold size of 300 nm [*Georgii and Kleinjung*, 1967]. Although we believe the number concentration $D > 300$ nm to be much smaller than the total particle concentration, we do not have data to confirm this. For this reason we cannot address the effect of particle size on ice nucleation efficiency here.

2.1. Continuous Flow Diffusion Chamber

[8] IN concentrations were measured using one version of the Colorado State University field CFDC, described in detail elsewhere [*Rogers*, 1988; *Rogers et al.*, 2001]. The

Table 2. Parameters Used in Statistical Analysis

Parameter	Description	References
MCE (modified combustion efficiency)	Measure of fire combustion phase derived from excess CO_2 and CO concentrations. Larger values of MCE imply flaming, while lower values of MCE describe smoldering combustion. MCE was integrated over the time the drum was filled with smoke.	*McMeeking* [2008]; *Ward and Radke* [1993]
κ (hygroscopicity)	Describes the amount of water that is associated with a dry particle at a constant humidity. Hygroscopicity data were derived from cloud condensation nucleus measurements of the smokes.	*Petters and Kreidenweis* [2007]; M. D. Petters et al. (Cloud condensation nuclei activity of biomass burning aerosol, manuscript in preparation, 2009)
OC and EC (organic carbon and elemental carbon mass concentration)	$PM_{2.5}$ collected on a high-volume filter and analyzed using a Sunset Lab OC/EC analyzer.	*McMeeking* [2008]; *Sullivan et al.* [2008]
EFCO, EFCO2, EFNO, EFTHC (emission factors for CO, CO_2, NO, and total hydrocarbon)	Emitted mass of gas per unit mass of burned fuel.	*McMeeking* [2008]
Inorganic ions (Na^+, K^+, NH_4^+, Ca^{2+}, Mg^{2+}, Cl^-, SO_4^{2-}, NO_2^-)	$PM_{2.5}$ collected on a nylon filter and analyzing water extracts with ion chromatography.	
Max energy	Maximum fire energy derived from thermocouple that was placed on top of the exhaust stack.	*McMeeking* [2008]
Percent moisture	Moisture content determined setting aside a certain amount of fuel before the burn and weighing it before and after several days of drying inside a humidity-controlled chamber.	*McMeeking* [2008]
Burned fuel mass	Total mass placed on fuel bed.	*McMeeking* [2008]
Ash fraction	Remaining mass after the burn divided by the burned fuel mass.	*McMeeking* [2008]
Inorganic mass	Sum of inorganic ion masses.	
OC fraction, EC fraction, inorganic fractions	Mass of component divided by sum of all ions, OC and EC.	

CFDC consists of two vertically oriented concentric copper tubes (an inner wall and an outer wall), forming an annular gap of ~1.1 cm through which the sample aerosol flows. Prior to measurements, a coating of ice ~100 μm thick is formed on each wall by pumping water through the chamber, which is cooled to −25°C. The temperatures of the walls are then adjusted to reach operating conditions. The sample flow passes through the annular gap in the CFDC, constrained in a laminar flow between two sheath flows. The temperatures of the inner and outer walls and the position of the sample lamina determine the processing temperature and relative humidity of the sampled particles. Processing conditions were determined from the formulas given by *Rogers* [1988] using the saturation vapor pressure parameterization over water and ice from *Buck* [1981] (e_{w3} and e_{i1} from *Buck* [1981, Table 2]).

[9] The aerosol is exposed to the set point temperature and water supersaturation for 4–5 s. In the lower third of the instrument, the inner and outer walls are both cooled to the cold wall temperature. This causes the humidity profile to relax to ice saturation, evaporating cloud droplets that may have formed under supersaturated water conditions but retaining ice crystals. At the outlet of the instrument, an optical particle counter (OPC) (CLiMET model 3100) measures size-resolved particle number concentrations. Those particles which have grown to sizes with optical diameters >2 μm are presumed to be ice on the basis of previous tests. To avoid misclassification of supermicron aerosol particles as IN, an impactor with a 1.3 μm cut size is located in the inlet line to the CFDC. It is possible that particles larger than 1.3 μm may serve preferentially as ice nuclei, and if so, our IN measurements represent a lower estimate.

[10] In a typical experiment the aerosol temperature was kept constant while the relative humidity was gradually increased from 96% to 115%, with respect to the saturation vapor pressure of supercooled liquid water, over a period of 15–20 min. Hereafter, we will use the term SS_w = RH-100% to denote the supersaturation with respect to supercooled liquid water. In addition to the sample measurements, reference scans were performed using 100 nm dried ammonium sulfate particles generated from aqueous solution using a constant output atomizer (TSI, model 3076). Ammonium sulfate droplets do not freeze heterogeneously

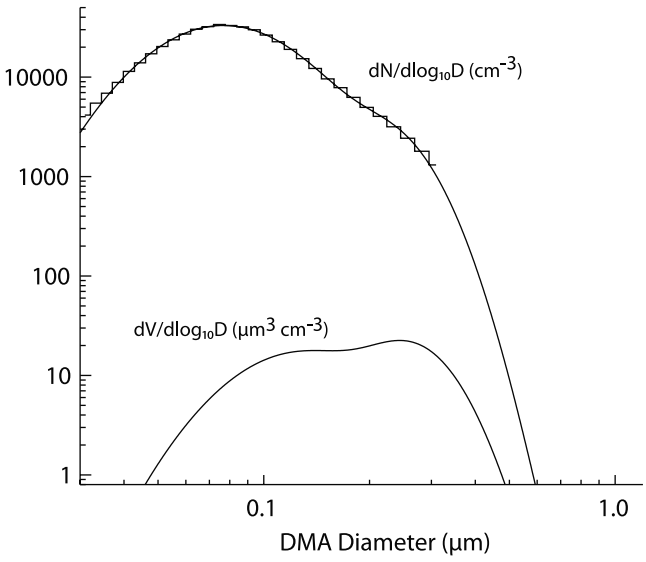

Figure 2. Example number particle size distribution obtained from the combustion of Douglas fir branches with needles (histogram). The solid line corresponds to a bimodal fit to the data and is also shown as volume weighted distribution ($dV/d\log_{10}D$).

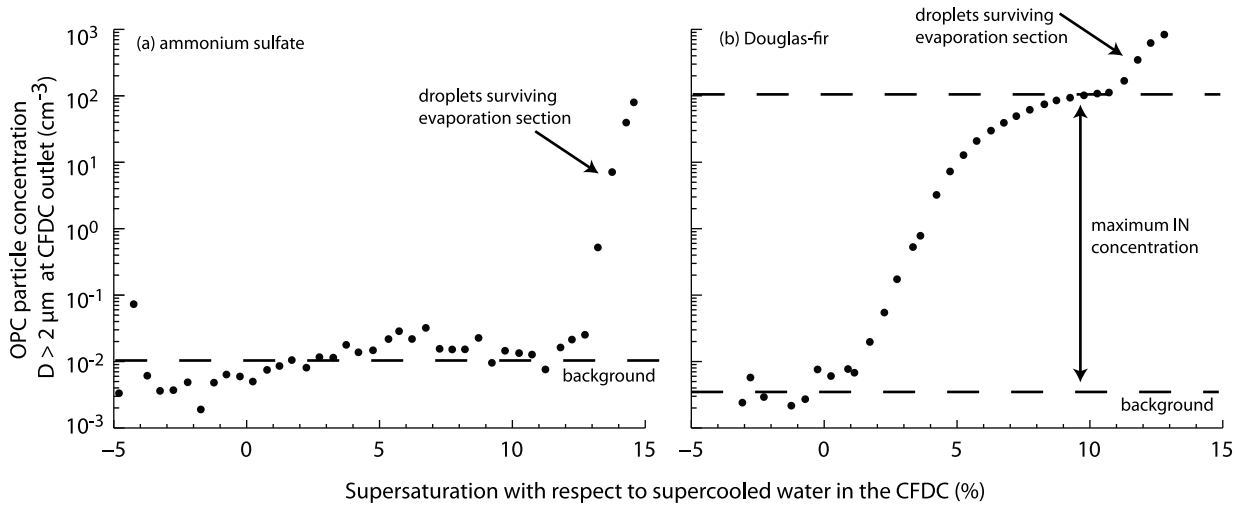

Figure 3. (a) Activation curves for ammonium sulfate and (b) emissions from the combustion of Douglas fir branches with needles. Total particle number concentrations entering the CFDC during the Douglas fir burn were ~15,000 cm^{-3}.

at temperatures warmer than approximately −36°C, and thus any growth of these particles can only be due to water uptake and cloud condensation nucleus activation. At very high supersaturations with respect to water, ammonium sulfate particles grow to sizes that are too large to be shrunk in the evaporation region below the size cut point designated for ice (>2 μm). The SS_w at which unfrozen cloud droplets formed on ammonium sulfate particles are detected at sizes greater than the OPC threshold defines the upper limit of detection of ice particles using this technique.

[11] Figure 3a shows an example SS_w scan for ammonium sulfate. Plotted are the OPC concentrations for particles larger than 2 μm. Points are averaged values over finite SS_w intervals with 0.5% bin width. During normal operation of the instrument, ice crystals can flake off the iced walls, leading to spurious counts in the OPC. These events define the background against which ice formation can be detected, and this correction is defined by the OPC concentration at $SS_w < 0\%$. These background concentrations varied from day to day, typically no lower than 0.002 cm^{-3} and, in some cases, exceeded 0.1 cm^{-3}. Background counts were not determined in particle-free air, and in the case of the higher background concentrations, some contributions came from aerosol counts. This was due to operation of the OPC on a higher gain setting, which caused aerosol concentrations to bleed into the larger-sized bins. This aerosol contribution was constant with SS_w and raised our limit of detection, as discussed further in section 2.2. During the SS_w scan for ammonium sulfate (Figure 3a) the background is nearly constant until $SS_w > 10\%$. Point-to-point fluctuations are likely caused by Poisson counting statistics. Each point corresponds to an average of ~30 s of raw data. At background concentrations of 10 L^{-1} and a CFDC sample flow rate of 1 L min^{-1}, this corresponds to ~5 raw counts per point plotted, with a counting error of $\sqrt{5}/5$, corresponding to a relative uncertainty of ~90%, assuming 2 standard deviations of variability around the mean value [*Snider and Petters*, 2008]. Most points are within a factor of 2 of this mean value. The sharp increase in detected particles at $SS_w > 10\%$ is not ice formation but is due to the inability of the evaporation region to shrink the droplets below the threshold diameter. Figure 3b shows a typical SS_w scan for a biomass burning sample. Below water saturation, the measured counts define the background. At $SS_w > 2\%$ the counts increase with SS_w, reaching a plateau of 100 cm^{-3} at $SS_w = 9\%$. In contrast to ammonium sulfate particles that do not freeze for $2\% < SS_w < 9\%$, this behavior demonstrates ice formation. At even higher humidities, a second increase in activated fraction is observed. In this region, biomass burning particles which have activated as droplets but have not frozen remain sufficiently large such that they are detected above the 2 μm cut size in the OPC. These data are not included as contributors to measured IN concentrations. The threshold where droplets survive the evaporation region varies between experiments, $9\% < SS_w < 13\%$. This is due to small fluctuations in the actual aerosol sample temperature (−30.4 ± 0.6°C) and small differences in the filling level of the CFDC during icing, which impacts iced length and/or ice growth time. We therefore examined each scan individually and determined the maximum IN concentration at the point where the slope is discontinuous.

[12] We expect that all input particles have been incorporated into cloud droplets in the instrument at $SS_w \sim 9\%$. That implies that all particles activate and form droplets in the instrument without the discrimination based on the peak supersaturation that is seen in naturally occurring clouds, where particles with dry diameter less than 60 nm generally do not activate and remain in the interstitial phase. Those particles, however, may still be incorporated into cloud droplets through Brownian diffusion to cloud droplets or through collection by settling hydrometeors, and therefore, we chose to include them in the CFDC measurement. Most importantly, however, we chose $SS_w \sim 9\%$ to accelerate the growth of droplets in the upper section of the instrument such that droplet diameters resemble those of cloud droplets in the atmosphere. Therefore, we capture the condensation/immersion freezing mode for all particles in the sample,

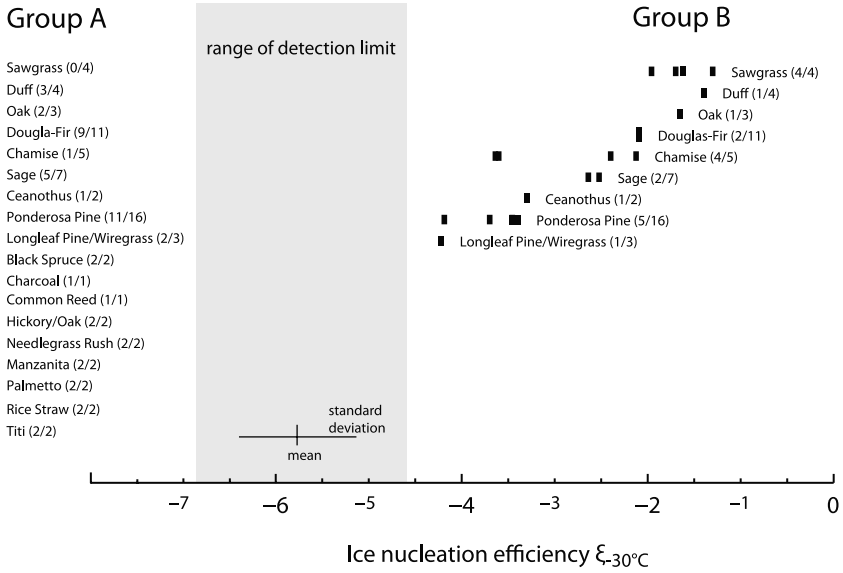

Figure 4. Ranked ice nucleation efficiency. Individual points indicate values for multiple burns. Parenthetical values (e.g., (0/4)) denote the number of samples in each group and the total number of samples. If two fuels are listed, a mixture of the two fuels was burned.

including those particles that may not form droplets in ambient cumulus clouds. Further, we focus on measurements at −30°C (as described further in section 2.2) and $SS_w \sim 9\%$ because we believe that under these conditions IN number concentrations will be greatest, therefore providing an upper limit estimate of potential emissions.

2.2. Ice Nucleation Efficiency Parameter

[13] To facilitate a simple but quantitative analysis of the freezing data, we define an ice nucleation efficiency parameter, ξ_T, as

$$\xi_T = \log_{10} m, \tag{1}$$

where m is the maximum activated fraction below the supersaturation where cloud droplets survive the evaporation region and T is temperature, fixed at −30°C. The activated fraction is obtained by subtracting the background frost counts from the OPC concentration (Figure 3b) and dividing by the concurrent total particle concentration measured by the CPC. This definition is tied to the operational capability of the CFDC. Nevertheless, as can be seen in Figure 3b, the measured IN concentration becomes independent of instrumental supersaturation at $SS_w \sim 9\%$. The limit of detection for ξ_T depends on the background counts and the total particle concentrations. For the 72 SS_w scans, particle concentrations ranged from 1000 to 20,000 cm^{-3}, with the majority of samples (n = 65) having concentrations exceeding 10,000 cm^{-3}. At T = −30°C and $N > 10{,}000$ cm^{-3} the vapor flux from the warm to the cold wall is sufficient to maintain equilibrium supersaturation against the growing water droplets. Further, at $SS_w > 11\%$ the drops grow large enough to not evaporate in the evaporation region. This demonstrates that water vapor is not limiting for ice detection. Calculated detection limits were $\xi_T = -5.6 \pm 0.6$ (mean and standard deviation), the minimum detection limit ξ_T was −6.8, and the maximum ξ_T was −4.6.

[14] Although we did not investigate the temperature dependence of ξ and limit our discussion to $\xi_{-30°C}$, it is likely that IN efficiency decreases with increasing temperature, similar to what has been observed for bacterial [*Rogers et al.*, 1987], mineral [*Vali*, 1994], and ambient IN [*Möhler et al.*, 2007]. Thus, data from this work should generally represent an upper limit of the fraction of submicron biomass burning active as condensation/immersion freezing nuclei at −30°C, if no coarse mode particles are present.

3. Results and Discussion

[15] Figure 4 ranks the sampled smokes by their average $\xi_{-30°C}$ for 72 SS_w scans, including multiple burns of the same fuel type. Typically, at least one replicate burn was conducted for each fuel type, although IN data were not obtained for all cases. For some of the fuels (chamise, ponderosa pine needles, and Douglas fir branches with needles), a larger number of multiple burns were performed to test the effect of burned fuel mass, fuel moisture, and combustion conditions on emission factors and on smoke sample properties. Fifty-one of the SS_w scans had no observed IN above the detection limit, and for clarity, these data are not plotted in Figure 4 but are represented by the parenthetical values in group A. These are likely not important for the regional ice nuclei budget, as will be discussed later. Among the samples that did exhibit measurable IN activity, $\xi_{-30°C}$ varied from −4.2 for the least active to −1.3 for the most active samples.

[16] To determine whether these $\xi_{-30°C}$ values are significant, we estimate the geographical area that may be affected by perturbed IN concentrations following an injection of emissions from a biomass burn. To do so, we use the

bottom-up approach to estimate emissions from biomass burning, following *Wiedinmyer et al.* [2006]:

$$EF_{IN} = B \times FBFB \times EF_{PM} \times NMR \times 10^{\xi}, \quad (2)$$

where EF_{IN} is the emission factor of ice nuclei in number per unit area burned, B is the fuel loading (mass of biomass per unit area), FBFB is the fraction of biomass fuel burned, EF_{PM} is the particulate matter mass emission factor (mass of aerosol per mass of biomass burned), NMR is the conversion factor from mass to number emissions (number of particles generated per unit mass of particulate matter emitted), and ξ is the log of the ice active fraction as defined above. For temperate forests and grasslands, B ranges from 1 to 10 kg m^{-2} [*Wiedinmyer et al.*, 2006], FBFB ranges from 0.3 for woody fuels to 0.9 for herbaceous fuels [*Wiedinmyer et al.*, 2006], EF_{PM} ranges from 1 to 20 g aerosol kg^{-1} fuel [*Chen et al.*, 2007; *Wiedinmyer et al.*, 2006], and $\xi_{-30°C}$ varies from less than -5.8 (average detection limit) to -1.3 for fuels that generate IN. The conversion from mass to number is somewhat uncertain. Aged smoke-impacted aerosol in Yosemite National Park ranges from 5 to 10×10^7 particles per μg aerosol [*McMeeking et al.*, 2005]. We found similar values during FLAME II, $1-30 \times 10^7$ particles per μg aerosol, from analyzing the mass to number ratios for smokes that were not vented through the stack but were diluted by filling the entire combustion chamber (chamber burns) and aged for several hours. On the basis of these data we assume that $1-30 \times 10^7$ particles per μg of smoke describe the number emissions reasonably well. We estimate the lower and upper bounds of EF_{IN} to be 5×10^6 and 3.4×10^{15} IN m^{-2} using the estimated minimum and maximum values for B, FBFB, EF_{PM}, NMR, and $\xi_{-30°C}$.

[17] Over what volume, or area, can these emissions disperse and contribute significantly to the observed IN concentrations? Assuming the plume dilutes unperturbed, i.e., there is no change in IN activity because of aging or a net loss in IN number because of coagulation, the dilution that can occur while maintaining concentrations exceeding a threshold IN_T is

$$\frac{EF_{IN} A_{burned}}{A_{spread} d} > IN_T, \quad (3)$$

where A_{burned} is the area burned, A_{spread} is the area the plume is distributed over, d is the assumed vertical depth of the dispersing plume, and IN_T is the threshold ice nuclei concentration that has to be exceeded by the spreading plume to maintain an impact. Typical number concentrations for samples collected on the ground or in the free troposphere and processed in the CFDC at $-30°C$ are ~ 10 L^{-1} [*Möhler et al.*, 2007]. For $IN_T = 10$ L^{-1} and a vertical plume width of 5 km, the ratio A_{spread}/A_{burned} can be computed from equation (3) and ranges from $\sim 7 \times 10^7$ to 0.1. Thus, a plume emanating from burning a square meter of biomass can potentially impact ice nuclei concentrations over an area up to 70 km^2 (7×10^7 m^2). However, no significant impact is expected if the IN efficiency is $\xi_{-30°C} = -6$ and lower emission factors are assumed. In that case the emitted IN concentrations are less than 10 L^{-1} in the plume directly above the burned area. Overall, the volume dilution factor scales directly with the ice nucleation efficiency. For a more realistic example, B = 10 kg m^{-2}, FBFE = 0.5, EF_{PM} = 10 g kg^{-1} fuel, NMR = 5×10^7 particles μg^{-1}, and $\xi_{-30°C} = -4$ (see pine burns in Figure 4), the expected area ratio reduces to 5000 m^2 per m^2 burned area; the true impact is likely less than that because not all burns of a fuel produced IN, and conditions that cause this variability are not accounted for in this model. In 1998, $\sim$18 million hectares of boreal forest burned [*Kasischke and Bruhwiler*, 2002], corresponding to an average of 3400 km^2 per week. Assuming an impact of 5000 km^2 per km^2 burned area and an implicit aerosol lifetime of $\sim$1 week, this corresponds to an average impacted area of approximately 4000 km $\times$ 4000 km in 1998, suggesting that fuels with $\xi_{-30°C} > -4$ may have significantly contributed to the regional IN budget.

[18] More than half of the fuels emitted no submicron IN above the detection limit, regardless of the number of burns. Other fuels, like ponderosa pine needles, produced significant IN for $\sim$30% of the burns. All burns of swamp saw grass produced significant IN concentrations. We point out, however, that the number of multiple burns was different for different fuels, and we cannot rule out the possibility that combustion of some of the fuels may emit IN under burning conditions that were not examined in this study. Of the fuels that generated IN, all displayed some variability in $\xi_{-30°C}$. Swamp saw grass, the fuel producing IN with the largest $\xi_{-30°C}$ values, showed the most consistent results, with IN generated during each of the four burns. The consistency of these results suggests that the fuel type is an important factor. Other fuels, however, showed greater variability. For example, emissions from the combustion of longleaf pine needles and Douglas fir branches with needles had measurable IN activity in only a few of the multiple burns; chamise combustion emissions gave $\xi_{-30°C}$ which ranged from about -4.2 to -1.2, and one burn was below the detection limit. It is worth noting that fuels from both the western and southeastern United States produced IN, and thus emissions of IN are not tied to a particular geographic region. These data suggest that factors in addition to fuel type, such as combustion conditions, fuel mass, and fuel moisture content, or, alternatively, other particles on the plant matter, may impact the emissions of IN, presumably by altering the chemical composition or the physical surface properties of the aerosol generated during the burn.

[19] As a first step in understanding the influences on observed $\xi_{-30°C}$, we performed statistical analyses using $\xi_{-30°C}$ as the variable describing IN activity. We divide the population into two groups: group A contains all samples with $\xi_{-30°C}$ below the detection limit ($n_A = 51$), while group B includes all samples with measurable $\xi_{-30°C}$ ($n_B = 21$). We then test whether certain measured properties, e.g., organic carbon mass fraction, aerosol hygroscopicity, etc., are related to IN emissions. Table 2 lists the variables we included in our analysis and gives a brief description of each. For the purpose of the following discussion we denote the tested parameter X. In this analysis, we only include samples with X above the detection limits in both group A and group B. We then examine whether the mean values of X differed significantly between groups A and B. This is accomplished by first calculating the mean and standard

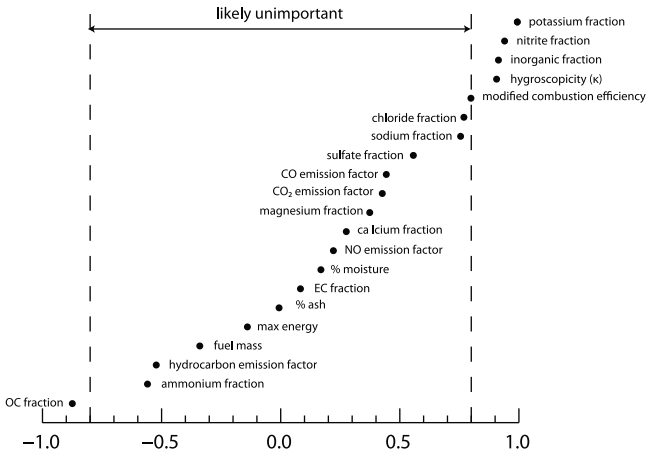

Figure 5. Significance coefficient for measured parameters. Coefficients outside the dashed lines are associated with whether the smoke did (positive) or did not (negative) emit IN above the limit of detection.

deviation of X in each population ($\mu_{X,\mathrm{A}}$, $\sigma_{X,\mathrm{A}}$, $\mu_{X,\mathrm{B}}$, $\sigma_{X,\mathrm{B}}$) and then calculating the t statistic for the two groups, with sample sizes, $n_{X,\mathrm{A}}$ and $n_{X,\mathrm{B}}$ [*Press et al.*, 1992, p. 616].

$$t = \frac{(\mu_{X,\mathrm{A}} - \mu_{X,\mathrm{B}})f^{0.5}}{\sqrt{\left[(n_{X,\mathrm{A}}-1)\sigma^2_{X,\mathrm{A}} + (n_{X,\mathrm{B}}-1)\sigma^2_{X,\mathrm{B}}\right]\left[1/n_{X,\mathrm{A}} + 1/n_{X,\mathrm{B}}\right]}}$$
$$f = n_{X,\mathrm{A}} + n_{X,\mathrm{B}} - 2. \quad (4)$$

From these data, we can then calculate the probability that $\mu_{X,\mathrm{A}}$ differs significantly from $\mu_{X,\mathrm{B}}$ [*Press et al.*, 1992, p. 229]:

$$P = 1 - I_{f/(f+t^2)}\left(\frac{f}{2}, \frac{1}{2}\right), \quad (5)$$

where P denotes the significance level at which the hypothesis that the means are equal is disproved and I_X is the incomplete beta function. Finally, we introduce the significance coefficient, S, defined as

$$S_X = \mathrm{sgn}(\mu_{X,\mathrm{B}} - \mu_{X,\mathrm{A}})P, \quad (6)$$

where sgn is the sign function. For example, if X is "organic mass fraction" and $S = -0.88$, there is an 88% probability that the mean for group B (samples that formed ice) is smaller than that for group A (samples that did not nucleate ice above the detection limit). The significance coefficient thus combines the likelihood that X is significantly different between the samples that do and do not produce IN with the direction of impact on IN being positive or negative. In typical statistical hypothesis testing, a significance value is assumed to delineate whether the null hypothesis that X was larger or smaller when comparing two populations is true or false. Here we do not assume a fixed significance value but report the level of significance at which a true/false claim may be made. However, for the following discussion, we choose a value of $|S_X| > 0.8$ as an indicator that X may play an important role in determining whether IN are generated. Figure 5 is a graphical representation of S_X for the parameters listed in Table 2. The region with $|S_X| < 0.8$ is indicated. Parameters that fall in this region are ash fraction, maximum fire energy, burned fuel mass, fuel moisture content, gas phase emission factors for NO, CO, CO_2, and hydrocarbons, water-soluble calcium, sodium, chloride, magnesium, and ammonium fraction, and, perhaps surprisingly, elemental carbon fraction.

[20] Figure 5 also shows positive significance for some inorganic water-soluble ions such as potassium fraction, nitrite fraction, or total water-soluble inorganic fraction. Further, aerosol hygroscopicity (κ), which describes the tendency of an aerosol to grow hygroscopically and form cloud droplets, is also significantly larger for smokes that produced IN. Since IN are generally considered to be water-insoluble [*Pruppacher and Klett*, 1997, p. 326], the data shown in Figure 5 are unlikely indicative of a causal relationship. Instead, this result may reflect underlying fuel compositional characteristics or process-related characteristics that govern the emissions of both water-soluble compounds and ice nuclei, and how these components mix in the aerosol phase.

[21] Organic carbon (OC) fractions are significantly lower in smokes that produced IN. This is plausible since organic carbon has been suggested to reduce heterogeneous ice nucleation ability of soot [*Möhler et al.*, 2005] and mineral dust particles [*Koehler*, 2007; *Möhler et al.*, 2008] at $T < -40°C$. Finally, modified combustion efficiency (MCE) is larger for samples that did nucleate ice than in the group that did not, suggesting that combustion conditions are also important. Flaming combustion, which is associated with higher combustion efficiencies, generally produces more soot and suppresses organic carbon formation [*McMeeking*, 2008]. Since elemental carbon mass fraction and IN emissions appear to be unrelated (Figure 5), we speculate that the presence of large fractions of organic carbon, produced during the smoldering fire phase, suppresses activity of potential ice nuclei, and thus the positive significance of MCE and the negative significance of organic carbon are connected.

[22] We caution against overinterpretation of the preceding statistical analyses. The significance coefficient is obtained by contrasting bulk properties of smokes between the group of smokes that did and did not generate IN. We intentionally limited the analysis to properties of the burned fuel, the fire, and the relative variability in smoke composition. However, it is unclear to what extent these bulk quantities apply to the properties of 1:100 or less of the particles formed by the fire. Therefore, we recommend that future studies also examine directly the composition of residuals of the particles that nucleated ice [e.g., *Cziczo et al.*, 2003; *Kreidenweis et al.*, 1998].

4. Conclusions

[23] This study investigated the ice nucleating ability of biomass burning particles generated from 21 different fuels. The majority of burns (51 out of 72) investigated did not produce particles that serve as condensation/immersion freezing IN above our instrumental detection limit. Of the fuels that did produce IN, swamp saw grass smoke exhibited the greatest IN fraction with ~1:100 particles

emitted serving as IN. The fact that some biomass burning particles were observed to heterogeneously nucleate ice supports the hypothesis that biomass burning particles impact aerosol-cloud interactions beyond increasing cloud condensation nuclei concentrations near sources. Because biomass burning emissions can both suppress warm rain processes and enhance ice nucleation, biomass burning may greatly affect cold cloud formation in smoke-affected regions, as suggested by *Lin et al.* [2006] and *Sassen and Khvorostyanov* [2008].

[24] Using a bottom-up emission estimate, we found that fuels with $\xi_{-30°C} > -4$ produce a large IN impact footprint of $\sim$5000 m^2 impacted per m^2 of vegetated surface burned. This suggests that biomass burning aerosols with specific chemical or physical properties affect the populations of particles involved in condensation/immersion freezing mode pathways of heterogeneous ice nucleation in the atmosphere on at least a regional scale. A statistical analysis contrasting bulk properties of smokes that did and did not nucleate IN suggests that IN emissions for the fuels we tested appear to be associated with low organic carbon fraction, high water-soluble ion content, and more flaming fire phase. Although this analysis cannot conclusively prove the underlying causal linkages between plant composition, fire behavior, aerosol chemical composition, and IN emissions, it suggests potential pathways that lead to IN production in fires that require further investigation.

[25] Last, we note that this study only considered the burning emissions from specific fuels on a small scale. Large-scale biomass burns that occur in wild and prescribed fires are capable of reaching higher temperatures than achieved in our burns and may have lower air-to-fuel ratios during combustion. This may impact combustion efficiencies and, in turn, IN emissions. Additionally, there is a possibility for dust, soil, and ash material to loft into the atmosphere during wild and prescribed fires [*Andreae et al.*, 2004; *Reid et al.*, 1998], and these particle types may impact the heterogeneous nucleation abilities of biomass burning emissions. In situ studies of the ice nucleation properties of particles in large-scale biomass burning plumes would be useful to gain a better understanding of the role of biomass burning particles in cold cloud formation.

[26] **Acknowledgments.** We acknowledge funding from the Joint Fire Science Program under Project JFSP 05-3-1-06. We also acknowledge support from the Department of Energy NICCR under grant MPC35TA-A, the National Aeronautics and Space Administration under grants NNG06GF00G and NNG04GR44G, and the National Science Foundation under grant NSF ATM-0521643. G.R.M. was supported by a U.S. Graduate Research Environmental Fellowship (GREF) funded by the U.S. Department of Energy's Global Change Education Program. We thank Wei-Min Hao and William Malm for their key roles in organizing the FLAME study. We thank all supporting members of the FLAME II team, particularly staff at the USDA Forest Service Fire Sciences Laboratory in Missoula. We thank Mike Chandler, Joey Chong, Guenter Engling, Eric Garrell, Grizelle Gonzales, Sue Grace, Jennifer Hinkley, Randi Jant, Sheah Mucci, Rachael Moore, Robert Olson, Kenneth Outcalt, Jim Reardon, Kevin Robertson, Pauline Spain, and David Weise for collecting the fuel samples for the project. We thank two anonymous reviewers for constructive criticism that helped us improve this manuscript.

References

Abbatt, J. P. D. (2003), Interactions of atmospheric trace gases with ice surfaces: Adsorption and reaction, *Chem. Rev.*, *103*(12), 4783–4800, doi:10.1021/cr0206418.

Andreae, M. O. (1991), Biomass burning: Its history, use, and distribution and its impact on environmental quality and global climate, in *Global Biomass Burning: Atmospheric, Climatic, and Biospheric Implications*, edited by J. S. Levine, pp. 1–21, MIT Press, Cambridge, Mass.

Andreae, M. O., D. Rosenfeld, P. Artaxo, A. A. Costa, G. P. Frank, K. M. Longo, and M. A. F. Silvia-Dias (2004), Smoking rain clouds over the Amazon, *Science*, *303*(5662), 1337–1342, doi:10.1126/science.1092779.

Buck, A. L. (1981), New equations for computing vapor pressure and enhancement factor, *J. Appl. Meteorol.*, *20*(12), 1527–1532, doi:10.1175/1520-0450(1981)020<1527:NEFCVP>2.0.CO;2.

Chakrabarty, R. K., H. Moosmüller, M. A. Garro, W. P. Arnott, J. Walker, R. A. Susott, R. E. Babbitt, C. E. Wold, E. N. Lincoln, and W. M. Hao (2006), Emissions from the laboratory combustion of wildland fuels: Particle morphology and size, *J. Geophys. Res.*, *111*, D07204, doi:10.1029/2005JD006659.

Chen, L. W. A., H. Moosmüller, W. P. Arnott, J. C. Chow, J. G. Watson, R. A. Susott, R. E. Babbitt, C. E. Wold, E. N. Lincoln, and W. M. Hao (2007), Emissions from laboratory combustion of wildland fuels: Emission factors and source profiles, *Environ. Sci. Technol.*, *41*(12), 4317–4325, doi:10.1021/es062364i.

Cozic, J., S. Mertes, B. Verheggen, D. J. Cziczo, S. J. Gallavardin, S. Walter, U. Baltensperger, and E. Weingartner (2008), Black carbon enrichment in atmospheric ice particle residuals observed in lower tropospheric mixed phase clouds, *J. Geophys. Res.*, *113*, D15209, doi:10.1029/2007JD009266.

Cziczo, D. J., P. J. DeMott, C. Brock, P. K. Hudson, B. Jesse, S. M. Kreidenweis, A. J. Prenni, J. Schreiner, D. S. Thomson, and D. M. Murphy (2003), A method for single particle mass spectrometry of ice nuclei, *Aerosol Sci. Technol.*, *37*(5), 460–470, doi:10.1080/02786820300976.

DeMott, P. J. (1990), An exploratory study of ice nucleation by soot aerosols, *J. Appl. Meteorol.*, *29*(10), 1072–1079, doi:10.1175/1520-0450(1990)029<1072:AESOIN>2.0.CO;2.

Diehl, K., and S. K. Mitra (1998), A laboratory study of the effects of a kerosene-burner exhaust on ice nucleation and the evaporation rate of ice crystals, *Atmos. Environ.*, *32*(18), 3145–3151, doi:10.1016/S1352-2310(97)00467-6.

Diehl, K., M. Simmel, and S. Wurzler (2006), Numerical sensitivity studies on the impact of aerosol properties and drop freezing modes on the glaciation, microphysics, and dynamics of clouds, *J. Geophys. Res.*, *111*, D07202, doi:10.1029/2005JD005884.

Diehl, K., M. Simmel, and S. Wurzler (2007), Effects of drop freezing on microphysics of an ascending cloud parcel under biomass burning conditions, *Atmos. Environ.*, *41*(2), 303–314, doi:10.1016/j.atmosenv.2006.08.011.

Dymarska, M., B. J. Murray, L. M. Sun, M. L. Eastwood, D. A. Knopf, and A. K. Bertram (2006), Deposition ice nucleation on soot at temperatures relevant for the lower troposphere, *J. Geophys. Res.*, *111*, D04204, doi:10.1029/2005JD006627.

Gavish, M., R. Popovitzbiro, M. Lahav, and L. Leiserowitz (1990), Ice nucleation by alcohols arranged in monolayers at the surface of water drops, *Science*, *250*(4983), 973–975, doi:10.1126/science.250.4983.973.

Georgii, H. W., and E. Kleinjung (1967), Relations between the chemical composition of atmospheric particles and the concentration of natural ice nuclei, *J. Rech. Atmos.*, *1*, 145–155.

Gorbunov, B., A. Baklanov, N. Kakutkina, H. L. Windsor, and R. Toumi (2001), Ice nucleation on soot particles, *J. Aerosol Sci.*, *32*(2), 199–215, doi:10.1016/S0021-8502(00)00077-X.

Intergovernmental Panel on Climate Change (2007), *Climate Change 2007: The Physical Science Basis. Contribution of Working Group I to the Fourth Assessment Report of the Intergovernmental Panel on Climate Change*, 996 pp., Cambridge Univ. Press, New York.

Karcher, B., O. Mohler, P. J. DeMott, S. Pechtl, and F. Yu (2007), Insights into the role of soot aerosols in cirrus cloud formation, *Atmos. Chem. Phys.*, *7*, 4203–4227.

Kasischke, E. S., and L. P. Bruhwiler (2002), Emissions of carbon dioxide, carbon monoxide, and methane from boreal forest fires in 1998, *J. Geophys. Res.*, *108*(D1), 8146, doi:10.1029/2001JD000461.

Koehler, K. (2007), The impact of natural dust aerosol on warm and cold cloud formation, Ph.D. thesis, 207 pp., Colo. State Univ., Fort Collins.

Koren, I., Y. J. Kaufman, L. A. Remer, and J. V. Martins (2004), Measurement of the effect of Amazon smoke on inhibition of cloud formation, *Science*, *303*(5662), 1342–1345, doi:10.1126/science.1089424.

Kreidenweis, S. M., Y. Chen, D. C. Rogers, and P. J. DeMott (1998), Isolating and identifying atmospheric ice-nucleating aerosols: A new technique, *Atmos. Res.*, *46*, 263–278, doi:10.1016/S0169-8095(97)00068-9.

Langer, G., C. Cooper, C. T. Nagamoto, and J. Rosinski (1978), Ice nucleation mechanisms of submicron monodispersed silver iodide, 1,5-dihydroxynaphthalene and phloroglucinol aerosol particles, *J. Appl.*

Meteorol., *17*(7), 1039–1048, doi:10.1175/1520-0450(1978)017<1039:INMOSM>2.0.CO;2.

Lin, J. C., T. Matsui, R. A. Pielke, and C. Kummerow (2006), Effects of biomass burning-derived aerosols on precipitation and clouds in the Amazon Basin: A satellite-based empirical study, *J. Geophys. Res.*, *111*, D19204, doi:10.1029/2005JD006884.

McFarquhar, G. M., and S. G. Cober (2004), Single-scattering properties of mixed-phase Arctic clouds at solar wavelengths: Impacts on radiative transfer, *J. Clim.*, *17*(19), 3799–3813, doi:10.1175/1520-0442(2004)017<3799:SPOMAC>2.0.CO;2.

McFarquhar, G. M., G. Zhang, M. R. Poellot, G. L. Kok, R. Mccoy, T. Tooman, A. Fridlind, and A. J. Heymsfield (2007), Ice properties of single-layer stratocumulus during the Mixed-Phase Arctic Cloud Experiment: 1. Observations, *J. Geophys. Res.*, *112*, D24201, doi:10.1029/2007JD008633.

McMeeking, G. (2008), The optical, chemical, and physical properties of aerosol and gases emitted by laboratory combustion of wildland fuels, Ph.D. thesis, 312 pp., Colo. State Univ., Fort Collins.

McMeeking, G. R., S. M. Kreidenweis, C. M. Carrico, T. Lee, J. L. Collett, and W. C. Malm (2005), Observations of smoke-influenced aerosol during the Yosemite Aerosol Characterization Study: Size distributions and chemical composition, *J. Geophys. Res.*, *110*, D09206, doi:10.1029/2004JD005389.

Möhler, O., C. Linke, H. Saathoff, M. Schnaiter, R. Wagner, A. Mangold, M. Kramer, and U. Schurath (2005), Ice nucleation on flame soot aerosol of different organic carbon content, *Meteorol. Z.*, *14*(4), 477–484, doi:10.1127/0941-2948/2005/0055.

Möhler, O., P. J. DeMott, G. Vali, and Z. Levin (2007), Microbiology and atmospheric processes: The role of biological particles in cloud physics, *Biogeosciences*, *4*(6), 1059–1071.

Möhler, O., S. Benz, H. Saathoff, M. Schnaiter, R. Wagner, J. Schneider, S. Walter, V. Ebert, and S. Wagner (2008), The effect of organic coating on the heterogeneous ice nucleation efficiency of mineral dust aerosols, *Environ. Res. Lett.*, *3*(2), 025007, doi:10.1088/1748-9326/3/2/025007.

Park, R. J., D. J. Jacob, and J. A. Logan (2007), Fire and biofuel contributions to annual mean aerosol mass concentrations in the United States, *Atmos. Environ.*, *41*(35), 7389–7400, doi:10.1016/j.atmosenv.2007.05.061.

Petters, M. D., and S. M. Kreidenweis (2007), A single parameter representation of hygroscopicity growth and cloud condensation nucleus activity, *Atmos. Chem. Phys.*, *7*, 1961–1971.

Prenni, A. J., P. J. DeMott, C. F. Rogers, S. M. Kreidenweis, G. M. McFarquhar, G. Zhang, and M. R. Poellot (2009), Ice nuclei characteristics from M-PACE and their relation to ice formation in clouds, *Tellus, Ser. B*, *61*(2), 436–448.

Press, W. H., S. A. Teukolky, W. T. Vetterling, and B. P. Flannery (1992), *Numerical Recipes in C: The Art of Scientific Computing*, 2nd ed., Cambridge Univ. Press, Cambridge, U. K.

Pruppacher, H. R., and J. R. Klett (1997), *Microphysics of Clouds and Precipitation*, 976 pp., Kluwer Acad., Dordrecht, Netherlands.

Reddy, M. S., and O. Boucher (2004), A study of the global cycle of carbonaceous aerosols in the LMDZT general circulation model, *J. Geophys. Res.*, *109*, D14202, doi:10.1029/2003JD004048.

Reid, J. S., P. V. Hobbs, R. J. Ferek, D. R. Blake, J. V. Martins, M. R. Dunlap, and C. Liousse (1998), Physical, chemical, and optical properties of regional hazes dominated by smoke in Brazil, *J. Geophys. Res.*, *103*(D24), 32,059–32,080, doi:10.1029/98JD00458.

Robertson, A., J. Overpeck, D. Rind, E. Mosley-Thompson, G. Zielinski, J. Lean, D. Koch, J. Penner, I. Tegen, and R. Healy (2001), Hypothesized climate forcing time series for the last 500 years, *J. Geophys. Res.*, *106*(D14), 14,783–14,803, doi:10.1029/2000JD900469.

Rogers, D. C. (1988), Development of a continuous flow thermal gradient diffusion chamber for ice nucleation studies, *Atmos. Res.*, *22*, 149–181, doi:10.1016/0169-8095(88)90005-1.

Rogers, J. S., R. E. Stall, and M. J. Burke (1987), Low-temperature conditioning of the ice nucleation active bacterium, *Erwinia herbicola*, *Cryobiology*, *24*(3), 270–279, doi:10.1016/0011-2240(87)90030-7.

Rogers, D. C., P. J. DeMott, S. M. Kreidenweis, and Y. L. Chen (2001), A continuous-flow diffusion chamber for airborne measurements of ice nuclei, *J. Atmos. Oceanic Technol.*, *18*(5), 725–741, doi:10.1175/1520-0426(2001)018<0725:ACFDCF>2.0.CO;2.

Sassen, K., and V. I. Khvorostyanov (2008), Cloud effects from boreal forest fire smoke: Evidence for ice nucleation from polarization lidar data and cloud model simulations, *Environ. Res. Lett.*, *3*(2), 025006, doi:10.1088/1748-9326/3/2/025006.

Snider, J. R., and M. D. Petters (2008), Optical particle counter measurements of marine aerosol hygroscopic growth, *Atmos. Chem. Phys.*, *8*, 1949–1962.

Sullivan, A. P., A. S. Holden, L. A. Patterson, G. R. McMeeking, W. C. Malm, W. M. Hao, C. E. Wold, and J. L. Collett (2008), A method for smoke marker measurements and its potential application for determining the contribution of biomass burning from wildfires and prescribed fires to ambient PM2.5 organic carbon, *J. Geophys. Res.*, *113*, D22302, doi:10.1029/2008JD010216.

Vali, G. (1985), Nucleation terminology, *Bull. Am. Meteorol. Soc.*, *66*(11), 1426–1427.

Vali, G. (1994), Freezing rate due to heterogeneous nucleation, *J. Atmos. Sci.*, *51*(13), 1843–1856, doi:10.1175/1520-0469(1994)051<1843:FRDTHN>2.0.CO;2.

Vonnegut, B. (1947), The nucleation of ice formation by silver iodide, *J. Appl. Phys.*, *18*(7), 593–595, doi:10.1063/1.1697813.

Ward, D. E., and L. E. Radke (1993), Emission measurements from vegetation fires: A comparative evaluation of methods and results, edited by P. J. Crutzen and J. G. Goldammer, in *Fire in the Environment. The Ecological, Atmospheric and Climatic Importance of Vegetation Fires*, pp. 53–76, John Wiley, New York.

Wiedinmyer, C., B. Quayle, C. Geron, A. Belote, D. McKenzie, X. Y. Zhang, S. O'Neill, and K. K. Wynne (2006), Estimating emissions from fires in North America for air quality modeling, *Atmos. Environ.*, *40*(19), 3419–3432, doi:10.1016/j.atmosenv.2006.02.010.

Yu, H., et al. (2006), A review of measurement-based assessments of the aerosol direct radiative effect and forcing, *Atmos. Chem. Phys.*, *6*, 613–666.

Zuidema, P., B. Baker, Y. Han, J. Intrieri, J. Key, P. Lawson, S. Matrosov, M. Shupe, R. Stone, and T. Uttal (2005), An arctic springtime mixed-phase cloudy boundary layer observed during SHEBA, *J. Atmos. Sci.*, *62*(1), 160–176, doi:10.1175/JAS-3368.1.

C. M. Carrico, J. L. Collett Jr., P. J. DeMott, S. M. Kreidenweis, E. Levin, M. D. Petters, A. J. Prenni, and A. P. Sullivan, Department of Atmospheric Science, Colorado State University, Campus Delivery 1371, Fort Collins, CO 80523-1371, USA. (petters@atmos.colostate.edu)

G. R. McMeeking, Center for Atmospheric Science, University of Manchester, Simon Building, Oxford Road, Manchester M13 9PL, UK.

H. Moosmüller, Desert Research Institute, Nevada System of Higher Education, 2215 Raggio Parkway, Reno, NV 89512, USA.

M. T. Parsons, Departments of Chemistry and Electrical Engineering, University of Alberta, 2036 Main Mall, Edmonton, AB T6G 2G2, Canada.

C. E. Wold, Fire Sciences Laboratory, U.S. Department of Agriculture Forest Service, P.O. Box 8089, Missoula, MT 59807, USA.